View metadata, citation and similar papers at core.ac.uk
brought to you by CORE
provided by Ghent University Academic Bibliography

The Role of Radicals in UV-Initiated Post-Plasma Grafting of PCL: an EPR Study

***Hendrik De Cooman*[1,2,#], *Tim Desmet*[3], *Freddy Callens*[1,*], *Peter Dubruel*[3]**

Title running head

Radicals in PCL Post-Plasma Grafting

Footnotes

[1] *Department of Solid State Sciences, Ghent University, Krijgslaan 281-S1, 9000 Gent, Belgium.*

[2] *Center for Molecular Modeling, Ghent University, Technologiepark 903, B-9052 Zwijnaarde, Belgium.*

[3] *Department of Organic Chemistry, Polymer Chemistry and Biomaterials Research Group, Faculty of Sciences, Ghent University, Krijgslaan 281, 9000 Gent, Belgium*

[#] Postdoctoral Fellow of the Fund for Scientific Research – Flanders (F.W.O. – Vlaanderen)

[*] Corresponding author. Tel: +32 9 264 43 52. Fax: +32 9 264 49 96. E-mail: Freddy.Callens@ugent.be.

Abstract

Electron paramagnetic resonance (EPR) measurements were performed on poly-ε-caprolactone (PCL) films at different stages of the post-plasma grafting process. PCL films prepared by solvent casting (SC) or electrospinning (ESP) yield very similar EPR spectra after Ar-plasma treatment and subsequent exposure to air, but the EPR signal is much stronger in the PCL-ESP films. The free radicals appear to be mainly, and possibly exclusively, oxygen-centered. The radicals generated by UV irradiation in PCL-ESP films were studied *in situ* with EPR, using a UV-LED (λ = (285 ± 5) nm). Their EPR spectrum is distinctly different from the plasma-induced signal, indicative of carbon-centered radicals, and appears to be independent of the plasma pre-treatment. UV-induced homolytic splitting of (hydro)peroxide bonds was not observed. Both the plasma- and UV-induced radicals decay at room temperature (RT), even in an inert atmosphere.

This study demonstrates the potential of electrospun films and UV-LEDs for the study of plasma- and UV-generated free radicals with EPR in polyesters, and raises questions with respect to the validity of some generally accepted molecular mechanisms underpinning the post-plasma grafting technique for polyesters.

Key words

Polyesters, photopolymerization, ESR/EPR, electrospinning, peroxides.

1. Introduction

In modern biomedical technology surface modification is of crucial importance.[1] Among the many different techniques available for the manipulation of polymers, the use of non-thermal plasma has demonstrated great potential, especially in the field of tissue engineering.[2-4] Plasma treatments can be subdivided in different categories, based on the application of the plasma. In the case of *direct plasma treatment*, the polymer is exposed to a gas-discharge, mostly to improve the wettability of the surface. In this case, no additional modifications are made to the polymer after exposure to the plasma discharge. In *plasma polymerization,* the discharge is used to deposit thin polymeric films (referred to as plasma-polymers) from monomers. Finally, in the *post-plasma grafting* or *plasma grafting* technique, the plasma treatment pre-activates the surface by introducing functional groups, which are subsequently used as initiation sites for further grafting. Recently, some of the current authors reported on the controlled and successful post-plasma grafting of 2-aminoethyl methacrylate (AEMA) onto poly-ε-caprolactone (PCL).[5] The chemical structures of both PCL and AEMA are depicted in Figure 1.

A lot of research in this field has focused on the grafting efficiency or the biologically relevant properties of the modified surfaces such as cell adhesion and viability.[3,4,6-11] The number of studies investigating the proposed mechanisms explicitly is more limited. A working model has been suggested for the post-plasma grafting of acrylamide on a polyethylene (PE) surface by Suzuki *et al.*,[12] and seems to be generally accepted and used in literature, e.g. also for the grafting of acrylic acid on PCL[6] or poly(ethylene terephthalate)[13] films and on silicone rubber membranes[14]. However, not all aspects of this model appear to be equally well supported by experimental evidence and it is unclear if such generalizations are

warranted. Assessing, improving and extending the working model is important, as knowledge of the molecular mechanisms may offer new insights and reveal possibilities for optimization of the post-plasma grafting technique.

Figure 2 shows the general scheme of the working model, applied to the grafting of AEMA onto PCL films. The plasma discharge induces free radicals on the PCL surface, for example via hydrogen abstraction, which subsequently react with the oxygen in an ambient atmosphere[6,7,15] or pure oxygen[13] to form peroxyl radicals:

$$R\text{-}H \rightarrow R^{\bullet} + H^{\bullet} \quad (1)$$

$$R^{\bullet} + O_2 \rightarrow R\text{-}O\text{-}O^{\bullet} \quad (2)$$

The latter yield peroxides via recombination/cross-linking reactions:

$$R\text{-}O\text{-}O^{\bullet} + (R')^{\bullet} \rightarrow R\text{-}O\text{-}O\text{-}R' \quad (3)$$

This is a hydroperoxide if R' represents a hydrogen atom. There is also a competing recombination/cross-linking reaction:

$$R^{\bullet} + R'^{\bullet} \rightarrow R\text{-}R' \quad (4)$$

The (hydro)peroxides serve as initiator sites for surface polymerization reactions resulting in the covalent immobilization of AEMA on the surface. Initiation is achieved by UV radiation[6,7,16] or thermal treatment[12-15,17-24], which lead to decomposition of the peroxides via homolytic scission, e.g.:

$$R\text{-}O\text{-}O\text{-}R' \rightarrow R\text{-}O^{\bullet} + {}^{\bullet}O\text{-}R' \quad (5)$$

UV light of 280 nm (4.35 eV) can also induce heterolytic scissions of the much stronger C-C, C-H and C-O bonds, but the resulting radicals are expected to be formed in much lower yields and typically assumed to be irrelevant for the grafting process.

The formation of peroxyl radicals by exposure to oxygen of plasma-treated polymers appears to be well established (Ref. 25 and references therein), but the molecular mechanisms of UV-induced grafting have, to the best of our knowledge, not been scrutinized. For example, there are other species (next to peroxides) that can initiate the grafting, such as free radicals.[8-11] Also note that this model is based on measurements on polyolefins like PE, which differ significantly in chemical composition from polyesters such as PCL.

Another remark to be made concerns the determination and optimization of the peroxide surface concentration. The most common approaches involve measuring the UV–Vis transmittance at 520 nm of 1-diphenyl-2-picrylhydrazyl (DPPH), a free radical which covalently bonds to peroxides at elevated temperatures,[12,17,19,26,27] or evaluation of the O/C ratio from the 1s core orbital signals of these atoms in X-ray Photoelectron Spectroscopy (XPS) spectra.[6,12] Both methods are, however, indirect and non-specific: free radicals such as DPPH may also react with free radicals at the specimen surface. This shortcoming is not remedied by the use of a blank sample (*i.e.* a sample that has not been subjected to an Ar-plasma treatment) reference since free radicals can be induced by the plasma treatment (in addition to the peroxides). The O1s/C1s ratio, on the other hand, does not allow distinguishing between the different oxygen-containing groups introduced by the plasma.

Free radicals, crucial intermediate products in both the plasma and UV treatment, provide a more direct source of information on the molecular reactions taking place. Electron

Paramagnetic Resonance (EPR), also known as Electron Spin Resonance (ESR), is particularly suited in this context as it is a non-destructive, highly sensitive spectroscopic technique that allows direct observation of free radicals and enables discrimination between different radical types and even between different conformations of the same radical species. EPR has been used to investigate radical formation in plasma-polymers[28] and free radicals after beta,[29,30] gamma[31-41] and plasma[42,43] irradiation of polyolefins. Peroxyl radical formation from plasma-induced radicals by reaction with ambient oxygen has been investigated in PE with EPR.[25] Also, interesting EPR results have very recently been obtained concerning UV grafting without plasma pre-functionalization.[44] However, no EPR studies on the radicals resulting from plasma treatment and subsequent UV irradiation of biodegradable polyesters seem to be available at the moment, even if this method is frequently employed for creating biofunctional surfaces.

The current work explores the possibilities that EPR offers for studying radical processes induced by plasma treatment and UV irradiation in the post-plasma grafting on biodegradable polyesters. It also aims at a better understanding of the molecular radical reactions and a further development of the working model. PCL is used as a model system.

2. Materials and Methods

2.1 Preparation and characterization of PCL samples

Samples were prepared either by solvent casting (SC) or electrospinning (ESP). These will be referred to as PCL-SC and PCL-ESP films, respectively. The PCL-SC films were casted onto a Petri dish from 20 ml of a 2 w/v % solution of PCL (Mw 70000-90000 Dalton, Sigma-

Aldrich) in tetrahydrofuran in an ambient atmosphere and subsequently stored in a vacuum oven overnight. PCL-ESP films were obtained from a 20 w/v% solution of PCL in a 2/1 chloroform/acetone solvent mixture on a home-made ESP device. A 10 ml needle was loaded with the polymer solution and connected to the dispenser. A tension of 15 kV was applied and the dispension speed was maintained at 10 ml/h. The distance to the collector was 15 cm.

Scanning electron microscopy (SEM) images of both films were obtained on a tabletop SEM device (desktop phenom microscope, Fei Company, the Netherlands). The samples were first coated with a layer of Au (≈ 20 nm) (Emitech K550X).

2.2 Plasma treatment

The PCL films were subjected to Ar plasma in a cylindrical dielectrical discharge plasma reactor (Model Femto, version 3, Diener Electronic, Germany) for 30 s. The Ar pressure was kept at 0.8 mbar and a power of 100 W was applied. These settings were employed and optimized in a previous study.[5]

2.3 *Ex-situ* UV irradiation (standard setup)

In the standard UV-initiated grafting procedure, plasma-pre-activated films were immersed in an aqueous, degassed AEMA (Polysciences) solution (pH ≈ 4.5) in a custom-made glass 6-well plate with a quartz cover, which was placed under a home-made UV device, equipped with 4 UV lamps (Sylvania, F15W/350, λ_{max} ≈ 350 nm) for 60 minutes, at approximately 10 cm from the lamps. The spectral distribution and the integrated optical output were determined by a 840-C power meter with a calibrated UV optical head (Newport), in combination with a calibrated QE65000 CCD-based spectrometer (Ocean

Optics). The total output was found to be approximately 3.7 mW per cm^2 in this setup, and the total power emitted at wavelengths below 310 nm about 50 μW per cm^2. The total power emitted at wavelengths below 300 nm (290 nm) could not be determined very accurately, but is roughly 15 μW per cm^2 (5 μW per cm^2), with an upper limit of 20 μW per cm^2 (10 μW per cm^2). Taking into account that the film absorbs approximately 10 % of the received power (based on *ex-situ* evaluation of the transmission and reflection of the film with a Varian Cary 500 spectrophotometer, equipped with an integrating sphere), 25 μW (8 μW) appears to be a reasonable estimate for the power in the $\lambda < 300$ nm ($\lambda < 290$ nm) region absorbed by a typical film sample (2 cm x 8 cm) in this setup.

2.4 EPR and *in-situ* UV irradiation

All EPR measurements were performed in a continuous-wave (CW) X-band (microwave frequency $\nu \approx 9.38$ GHz) EPR spectrometer (Bruker ESP300E) with a rectangular EPR cavity, in a He atmosphere and, unless stated otherwise, at 20 K. Clear signals were only obtained at low temperature (77 K or lower), but cooling below 20 K did not yield any further improvement. A modulation amplitude of 0.5 mT and a microwave power of 0.20 mW were applied, as these yielded a sufficiently strong signal-to-noise (S/N) ratio without deforming the spectrum. Magnetic field values were accurately determined with a Gauss meter and calibrated with DPPH ($g = 2.0036$). Unless stated otherwise, the spectra were not intensity-normalized. All spectra were normalized to a microwave frequency of 9.3800 GHz and binomially averaged to further suppress noise. The spectra were not baseline corrected but for every experiment, the empty sample tube or quartz rod was measured with identical parameter

settings in order to discriminate between background and sample signals. Spectral simulations were done with Easyspin[45] subroutines in Matlab (MathWorks, Inc., Natick, US-MA.). Following procedure is followed for i*n situ* annealing of samples: stopping the flow of cold He gas from the pre-dewar to the cavity by closing the needle valve, and letting warm He gas flow into the cavity. The temperature was constantly monitored by a thermocouple in the vicinity of the sample and never exceeded 295 K. Nominally, warming up to RT took less than 3 minutes.

PCL-SC films were cut into small pieces and stuffed into a teflon cup, which was inserted into the cavity. In the case of PCL-ESP samples, a piece of film (typical surface area of 2 cm x 8 cm and weight of 15 mg) was tightly wrapped (resulting sample thickness of about 0.5 mm) around the tip of a thin quartz rod (3 mm outer diameter), which was inserted directly into the cavity. This setup allowed *in-situ* UV irradiation of the samples through the irradiation grid (approximately 40 % transmission) in the cavity wall, and a more homogeneous deposition of UV energy in the sample was attained by rotation of the rod during irradiation. (The need for *in-situ* illumination will become clear in Section 3.) For this purpose, two UV-LEDs with peak emission wavelengths of (275 ± 5) nm (LED275) and (285 ± 5) nm (LED285) (Roithner Lasertechnik, Austria) were mounted on flexible wires. The LEDs were equipped with hemispherical lenses and have a typical output power of 0.5 mW. Based on similar measurements as for the UV lamps (Section 2.3), and taking into account the irradiation grid and the dimensions of the UV-LED and film, we estimate that the (multiply folded) film absorbs 5 - 10 % of the LED UV output in this setup (i.e. 25 - 50 μW) in the case of LED285 - the outer 0.25 mm of the sample absorbing about twice as much as the inner 0.25 mm. This is comparable to the total absorbed output in the $\lambda < 300$ nm region in the *ex-*

situ setup, but note that in the *in-situ* setup, only part of the film absorbs the radiation, due to the limited spread of the LED emission pattern.

2.5 XPS analysis

XPS measurements were performed on an ESCA S-probe VG monochromatized spectrometer with an Al K_α X-ray source (1486 eV). A survey scan spectrum was collected at a resolution of 1eV/point and relative elemental compositions of the material top layer (10 – 20 nm) determined from the peak-area ratios of the C and O 1s signals in CasaXPS software. The surveys were collected at nine different positions along the diameter of circular spin-coated PCL samples (texture comparable to that of SC films) of 18 mm diameter.

3. Results and Discussion

3.1 Structural characterization of the PCL films

Optical and SEM images of both PCL-SC and PCL-ESP films are presented in Figure 3. The PCL-SC films typically were thin, almost transparent, while the PCL-ESP films were white and had a more cotton-wool-like appearance. The SEM images indeed show that PCL-SC films are compact while the PCL-ESP films consist of many microfibers, indicating that the ESP processing of PCL was successful. The pores between the fibres are typically of the order of 10 μm, and air is removed before the plasma treatment, so that the Ar plasma should be able to penetrate all areas of the sample. We anticipated that the larger surface-to-volume

ratio should yield a higher relative yield of radicals in PCL-ESP films since plasma generates radicals mainly at the surface.[46]

3.2 Evaluation of the UV-LED system

To verify if the LEDs (as opposed to the UV lamps in the standard *ex-situ* setup, Section 2.3) are suitable for studying the UV-induced post-plasma grafting process, Ar-plasma-treated films were irradiated with the UV LEDs for one hour in an otherwise standard setup. The nitrogen content at the surface (used as indicator for the amount of covalently grafted poly-AEMA (pAEMA)) was subsequently determined by XPS using the 1s core signal of N. Table 1 summarizes the results of the survey spectra recorded at different positions along a diameter of these samples. Relative concentrations of around 3.2 ± 0.4 % and 4.9 ± 0.9 % are found for LED275 and LED285 respectively, which indicates that the grafting reaction is successful for both LEDs but considerably more efficient for LED285. Moreover, the values obtained for the latter are comparable to the 6 % obtained previously with the standard setup.[5] Therefore, all *in-situ* UV irradiation was performed with LED285.

3.3 EPR measurements

3.3.1 EPR monitoring of different stages in the grafting process

Figure 4 shows EPR spectra recorded on an ESP film at different stages, mimicking the standard grafting process: blank (Figure 4b), after Ar-plasma treatment followed by 10 minutes exposure to air at room temperature (RT) (Figure 4c), and after additional *in-situ* UV irradiation for 70 minutes at 20 K (Figure 4d). The reason for performing the UV irradiation

in situ at low temperature, rather than at RT as is done in the grafting process, will become apparent in Section 3.3.4.

A relatively faint EPR signal is present in the blank sample. The Ar-plasma treatment gives rise to a distinctly different EPR spectrum, typical of a randomly oriented powder with an axial or nearly axial symmetry. The effect of UV radiation is also clearly observable: while the low-field component appears to be largely unaffected, the high-field component grows stronger and broadens. These results demonstrate that the radicals generated by both Ar plasma and UV have well-resolved and distinctly different EPR signals. The dependency of these signals on the sample preparation and treatment is studied in the next sections.

3.3.2 Optimization of sample preparation and EPR setup

The plasma-induced EPR signal has largely decayed after 20 minutes at RT (Section 3.3.3). At 77 K (and, *a fortiori*, lower temperatures), however, it is perfectly stable. The spectra shown in the rest of this work were therefore recorded on samples that were transferred to a sealed box inside a Dewar at liquid nitrogen temperature immediately after Ar-plasma treatment for transport to the EPR spectrometer. Transfer from the Dewar to the EPR sample holder, insertion of the latter into the cavity and cooling to 20 K typically required between 2.5 and 3.5 minutes.

Blank and plasma-treated PCL-SC films yield EPR spectra similar to their PCL-ESP counterparts, as shown in Figure 5 for the plasma-treated samples. The limited differences are at least partially due to the proportionately higher contribution of the blank EPR signal in the PCL-SC films. The S/N ratio is, however, higher for the PCL-ESP films with a factor of about 6, even though their sample volume is smaller (see section 2.4): the EPR signal for

comparable sample volume would be at least an order of magnitude more intense for PCL-ESP films. The much higher radical yield can be rationalized in terms of the larger effective surface available for interaction with the Ar plasma. In addition, the EPR signal intensity of PCL-SC films exhibits relatively large fluctuations over different samples of comparable surface, while that of PCL-ESP films is more constant, and the possibility of using a smaller sample volume for PCL-ESP films allows for a convenient experimental setup for *in-situ* UV irradiation and for a more homogeneous absorption of UV light throughout the sample (see Section 2.4). Further experiments were therefore conducted on PCL-ESP films.

3.3.3 Ar-plasma-induced EPR signal

In Figure 6, the EPR spectra are shown of two samples of the same PCL-ESP film and of comparable surface, one blank and one subjected to the standard Ar-plasma treatment. The higher S/N ratio of the Ar-treated sample compared to spectrum c in Figure 4 is due to the shorter exposure to air at RT between the Ar-plasma treatment and transfer to the spectrometer cavity (less than 3 minutes versus 10 minutes). As before, the blank sample exhibits a single, weak and broad EPR line centered at g = 2.0033, typical of carbon-centered radicals. The Ar-induced EPR signal (spectrum c in Figure 6) differs entirely in both intensity and shape from the blank, indicating that the Ar plasma generates radicals in much higher quantity and of different types than those naturally present in the membrane.

The relatively high *g* factor (g = 2.0347) of the low-field EPR component reflects the presence of oxygen-centered radicals – which will also account for at least part of the higher-field component (g = 2.0028). A simulated EPR spectrum assuming the presence of only one type of randomly oriented oxygen-centered radicals with a Gaussian line profile is shown in

red in Figure 6. Considering the chemical and structural composition of the samples, there should be anisotropic hyperfine interactions with the nuclear spins of hydrogen atoms in the vicinity of the radical center, and one may expect a variety of geometrical conformations to occur for a particular radical species. These phenomena would result in anisotropic line broadening and a distribution of the principal *g* values, respectively, in the EPR spectrum. Taking such effects into account, and additionally assuming a mixture of Gaussian and Lorentzian line profiles, the green spectrum in Figure 6 can be obtained, which more closely matches experiment. Further improvements are possible, e.g. by assuming the presence of several species with distinct (but similar) *g* values. At any rate, it seems that a large portion of the EPR spectrum can be attributed to radicals with principal *g* values typical of an alkoxyl ($R_1R_2R_3$-C-O$^{\bullet}$) radical[47] or a peroxyl (R_1-O-O$^{\bullet}$) radical[25,32,34,35,48-50], the latter being the most obvious candidate. The absence of strong proton hyperfine interactions is also an argument in favor of this assignation, although beta proton hyperfine interactions of alkoxyl species strongly depend on the local conformation and can be small enough to match experiment.[47]

The Ar-induced signal is stable at 77 K, but decays relatively fast at RT, keeping essentially the same relative line intensities of the low- and high-field component. Therefore, all prominent radical species must have a similar decay rate. If an Ar-plasma-treated sample is exposed to air at RT for 20 minutes, the low-field line cannot be discerned anymore and the intensity of the high-field line is comparable to that of the blank signal. The same signal reduction with a comparable decay rate is observed when the sample is annealed to RT *in situ*, i.e. in a He atmosphere (Figure 7). Thus, radicals can decay via thermally driven recombination reactions without exposure to air. Note that *in situ* and *ex situ* annealing do not

result in identical temperature evolutions of a sample, but a qualitative comparison of the EPR signal decay rates seems justifiable.

3.3.4 UV-induced EPR signal

Figure 8 shows the EPR signal induced in a blank ESP film by 40 minutes *in-situ* UV irradiation at 20 K. It is a rather broad line with extended, low-intensity tails, centered at g = 2.0045 and a much higher intensity than the blank signal. The relatively small deviation of the g values from the free-electron value g_e indicates mainly, or exclusively, carbon-centered radicals are produced, while the large line width suggests a variety of radicals is formed, possibly including some with limited spin delocalization onto an oxygen atom, e.g. with a carbonyl group in the direct vicinity of the radical center. The lack of hyperfine structure in the spectrum indicates there are no strong proton hyperfine interactions but does not allow structural identification since these interactions strongly depend on the local geometrical conformation.

The UV-induced signal is stable at 77 K (and, *a fortiori*, 20 K) but has largely decayed after 20 minutes of RT annealing in a He atmosphere. The decay rate appears to be comparable to the decay rate of the plasma-induced signal, but more careful annealing studies would be required to draw conclusions in this respect. The sample temperature could influence the response to UV, but investigation of the EPR signal induced by UV radiation (be it *in situ* or *ex situ*) at RT is hampered by the fact that the decay rate is comparable to the UV-induced growth rate. Nevertheless, after 16 minutes of *in situ* UV irradiation at RT, a (very) faint UV-induced EPR component can be observed and its resemblance with the EPR signal induced at 20 K does suggest the same type of radicals are formed at 20 K and RT.

Based on this and the results presented in Section 3.3.5, *in-situ* UV irradiation at low temperature seems to be a valid approach for studying the UV-induced radicals in the actual grafting process.

3.3.5 Combined effect of Ar-plasma and UV

As demonstrated in Section 3.3.1, *in-situ* UV irradiation also generates radicals in samples that were first subjected to Ar-plasma treatment. Figure 9 shows that the EPR spectral components due to UV irradiation at 20 K of Ar-plasma-treated films and blank films are very similar in shape and intensity, suggesting that the type and amount of radicals formed by UV is largely independent on the preceding Ar-plasma exposure.

4. Conclusions

This study demonstrates that plasma- and UV-induced radicals at polymer surfaces can be studied with commercially available EPR equipment and UV-LEDs. This is interesting in the context of recent research on electrospun nanofibrous membranes for tissue engineering[46] and holds promise for further research, e.g. on the influence of the UV wavelength. Some relevant observations were also made with respect to the molecular mechanisms underlying the post-plasma grafting process of polyester membranes: (i) the plasma-induced oxygen-centered radicals are still present in significant amounts upon grafting initiation. (ii) The UV-induced species have a distinctly different EPR signature, typical of carbon-centered radicals. The oxygen-centered radicals that should result from the UV-induced homolytic splitting of (hydro)peroxide bonds (reaction (5)) in plasma-treated films were not observed. Also, no UV-induced conversion of the oxygen-centered radicals to alkyl radicals was detected, in contrast

to the findings of Siegel and Hedgpeth for gamma-irradiated polytetrafluoroethylene.[32] (iii) The UV-induced radical formation appears to be largely unaffected by the plasma pre-treatment. This indicates that UV generates radicals on the polymer chain and not (only) at the functional groups introduced by the plasma.

Some uncertainties should first be pointed out: (i) instable plasma- or UV-induced radicals may have decayed prior to the EPR measurements via recombination or fast reaction with oxygen. EPR experiments on plasma-treated samples without exposure to oxygen would be interesting but are not possible in our laboratories for the moment. (ii) The detected radical species may be secondary products. (iii) The UV-induced EPR signal was consistent in shape but variable in intensity throughout our experiments, both for blank and plasma-treated films. This inconsistency may well be relevant and worth further research.

Bearing these considerations in mind, we tentatively conclude that other processes than those typically considered in the working model of the post-plasma grafting technique (Figure 2), may (also) be important in the case of PCL films. In particular, the free radicals present upon grafting initiation and those continuously created on the polymer during UV exposure may affect the grafting process. This could explain the observed increase of the grafting efficiency with UV-exposure time.[5,7] Furthermore, the different polar groups introduced by the plasma treatment, which are known to increase the wettability of a hydrophobic polymer surface,[3] may not only act as initiator sites but also serve to enable a closer contact between the aqueous monomer solution and the pre-activated polymer surface.

Finally, we note that EPR measurements at higher microwave frequencies, more advanced electron magnetic resonance measurements (ENDOR (Electron Nuclear Double Resonance) and EIE (ENDOR-induced EPR),[31] and pulsed techniques) may help decompose the EPR spectra and identify the different contributing species.

Acknowledgements

The authors wish to thank Thomas Billiet of the Department of Organic Chemistry for practical assistance and prof. dr. Philippe Smet of the Lumilab research group at the Department of Solid State Sciences of Ghent University for his accurate determination of the spectrum and output power of the UV lamps and LEDs, and of the optical properties of the films. They also would like to acknowledge the UGent Multidisciplinary Research Partnership Nano- and biophotonics (2010-2015) for funding.

Citations

1. Roach, P.; Eglin, D.; Rohde, K.; Perry, C. C. J Mater Sci-Mater M 2007**,** 18, 1263-1277.

2. Goddard, J. M.; Hotchkiss, J. H. Prog Polym Sci 2007**,** 32, 698-725.

3. Desmet, T.; Morent, R.; De Geyter, N.; Leys, C.; Schacht, E.; Dubruel, P. Biomacromolecules 2009**,** 10, 2351-2378.

4. Siow, K. S.; Britcher, L.; Kumar, S.; Griesser, H. J. Plasma Processes Polym 2006**,** 3, 392-418.

5. Desmet, T.; Billiet, T.; Berneel, E.; Cornelissen, R.; Schaubroeck, D.; Schacht, E.; Dubruel, P. Macromol Biosci 2010, 10, 1484-1494.

6. Cheng, Z. Y.; Teoh, S. H. Biomaterials 2004, 25, 1991-2001.

7. Chong, M. S. K.; Lee, C. N.; Teoh, S. H. Mater Sci Eng C 2007**,** 27, 309-312.

8. Goddard, J. M.; Hotchkiss, J. H. Prog Polym Sci 2007**,** 32, 698-725.

9. Morent, R.; De Geyter, N.; Desmet, T.; Dubruel, P.; Leys, C. Plasma Processes Polym 2011**,** 8, 171-190.

10. Cheruthazhekatt, S.; Cernak, M.; Slavicek, P.; Havel, J. J Appl Biomed 2010**,** 8, 55-66.

11. Ma, P. X. Adv Drug Delivery Rev 2008**,** 60, 184-198.

12. Suzuki, M.; Kishida, A.; Iwata, H.; Ikada, Y. Macromolecules 1986**,** 19, 1804-1808.

13. Gupta, B.; Hilborn, J. G.; Bisson, I.; Frey, P. J Appl Polym Sci 2001**,** 81, 2993-3001.

14. Lee, S. D.; Hsiue, G. H.; Chang, P. C. T.; Kao, C. Y. Biomaterials 1996**,** 17, 1599-1608.

15. Baquey, C.; Palumbo, F.; Porte-Durrieu, M. C.; Legeay, G.; Tressaud, A.; d'Agostino, R. Nucl Instrum Methods Phys Res, Sect B **1999,** 151, 255-262.

16. Yao, C.; Li, X. S.; Neoh, K. G.; Shi, Z. L.; Kang, E. T. J Membr Sci 2008**,** 320, 259-267.

17. Lee, S. D.; Hsiue, G. H.; Kao, C. Y.; Chang, P. C. T. Biomaterials 1996**,** 17, 587-595.

18. Turmanova, S.; Minchev, M.; Vassilev, K.; Danev, G. J Polym Res 2008**,** 15, (4), 309-318.

19. Huang, C. Y.; Lu, W. L.; Feng, Y. C. Surf Coat Tech 2003**,** 167, 1-10.

20. Lewis, G. T.; Nowling, G. R.; Hicks, R. F.; Cohen, Y. Langmuir 2007**,** 23, 10756-10764.

21. Kinoshita, Y.; Kuzuhara, T.; Kirigakubo, M.; Kobayashi, M.; Shimura, K.; Ikada, Y. Biomaterials 1993**,** 14, 546-550.

22. Kinoshita, Y.; Kuzuhara, T.; Kirigakubo, M.; Kobayashi, M.; Shimura, K.; Ikada, Y. Biomaterials 1993**,** 14, 209-215.

23. Muir, B. W.; Barden, M. C.; Collett, S. P.; Gorse, A. D.; Monteiro, R.; Yang, L. Q.; McDougall, N. A.; Gould, S.; Maeji, N. J. Anal Biochem 2007**,** 363, 97-107.

24. Gupta, B.; Saxena, S.; Ray, A. J Appl Polym Sci 2008**,** 107, 324-330.

25. Kuzuya, M.; Kondo, S.; Sugito, M.; Yamashiro, T. Macromolecules 1998**,** 31, 3230-3234.

26. Shim, J. K.; Na, H. S.; Lee, Y. M.; Huh, H.; Nho, Y. C. J Membr Sci 2001**,** 190, 215-226.

27. Lee, S. D.; Hsiue, G. H.; Kao, C. Y. J Polym Sci, Part A: Polym Chem 1996**,** 34, 141-148.

28. Haupt, M.; Barz, J.; Oehr, C. Plasma Processes Polym 2008**,** 5, 33-43.

29. Al-Sheikhly, M.; Kasser, M. J.; Silverman, J. Macromolecules 2010**,** 43, 8862-8867.

30. Brunella, V.; Paganini, M. P. Magn Reson Chem 2011, 49, 562-569.

31. Murphy, D. M.; Bushell, J. A.; Claybourn, M.; Williams, H. E. Magn Reson Chem 2006**,** 44, 929-935.

32. Siegel, S.; Hedgpeth, H. J Chem Phys 1967, 46, 3904-3912.

33. Kuznetso, A. N.; Radtsig, V. A. Chem Phys Lett 1972, 17, 377-380.

34. Hori, Y.; Aoyama, S.; Kashiwabara, H. J Chem Phys 1981, 75, 1582-1584.

35. Seguchi, T.; Tamura, N. J Phys Chem 1973, 77, 40-44.

36. Hori, Y.; Shimada, S.; Kashiwabara, H. Polymer 1977, 18, 1143-1148.

37. Hori, Y.; Shimada, S.; Kashiwabara, H. Polymer 1977, 18, 151-154.

38. Hori, Y.; Fukunaga, Z.; Shimada, S.; Kashiwabara, H. Polymer 1979, 20, 181-186.

39. Hori, Y.; Shimada, S.; Kashiwabara, H. Polymer 1979, 20, 406-410.

40. Kashiwabara, H.; Hori, Y. Radiat Phys Chem 1981, 18, 1061-1066.

41. Reuben, J.; Mahlman, B. H. J Phys Chem 1984, 88, 4904-4906.

42. Kuzuya, M.; Niwa, J.; Ito, H. Macromolecules 1993, 26, 1990-1995.

43. Kuzuya, M.; Niwa, J.; Noguchi, T. Polym J 1995, 27, 251-255.

44. Berthelot, T.; Le, X. T.; Jégou, P.; Viel, P.; Boizot, B.; Baudin, C.; Palacin, S. Appl Surf Sci 2011, 257, 9473-9479 and references therein.

45. Stoll, S.; Schweiger, A. J Magn Reson 2006, 178, 42-55.

46. Zhong, S. P.; Zhang, Y. Z.; Lim, C. T. Wiley Interdiscip Rev Nanomed Nanobiotechnoly 2010, 2, 510-525.

47. Box, H. C.; Budzinski, E. E.; Freund, H.G. J Chem Phys 1984, 81, 4898-4902.

48 McCain, D. C.; Palke, W. E. J Magn Reson 1975, 20, 52-66.

49. Schlick, S.; Chamulitrat, W.; Kevan, L. J Phys Chem 1985, 89, 4278-4282.

50. Priest, V. V.; Cowan, D. L.; Yasar, H.; Ross, F. K. Phys Rev B 1991, 44, 9877-9882.

Tables

Table 1: Relative nitrogen concentration (in %) at the surface of spin-coated PCL films after post-plasma grafting of AEMA with UV-LEDS, as determined from XPS measurements using the 1s core signal of N.

	LED275	LED285
pos1	2.9	4.1
pos2	3.4	3.8
pos3	2.5	5.5
pos4	3.3	3.7
pos5	3.3	4.0
pos6	3.4	5.4
pos7	3.6	6.1
pos8	3.3	5.7
pos9	2.7	5.4
average	3.2	4.9
SD	0.4	0.9

Figures

Figure 1: Chemical structures of poly-ε-caprolactone (PCL) and 2-aminoethyl methacrylate (AEMA).

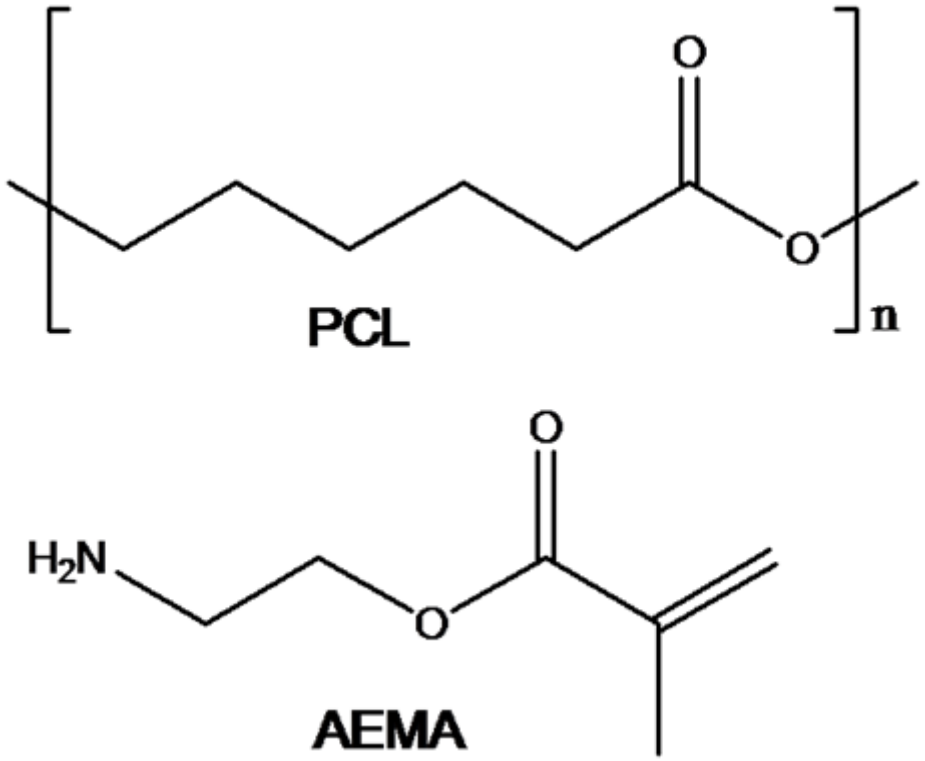

Figure 2: Working model for the post-plasma grafting technique, applied to the grafting of AEMA onto PCL.

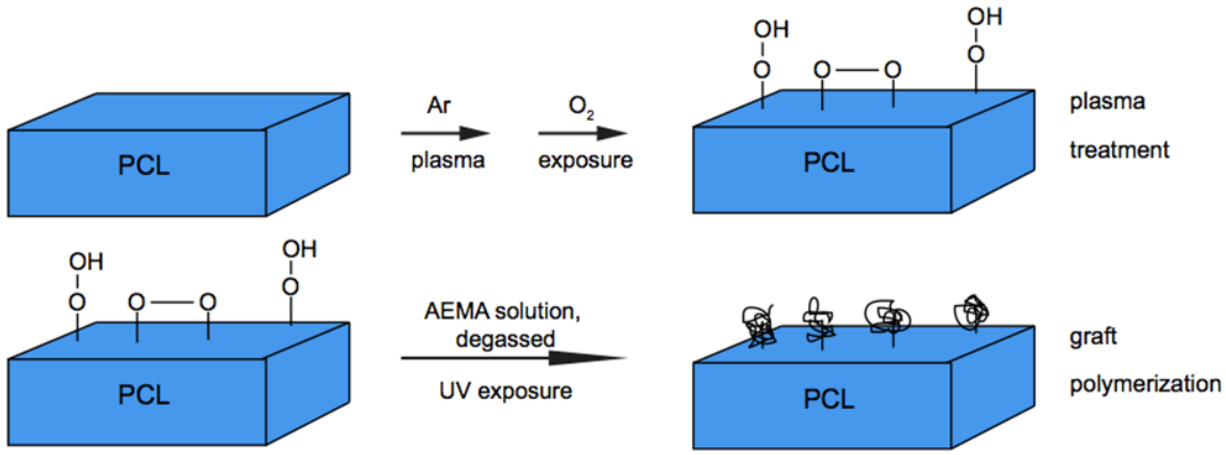

Figure 3: Optical (4x, left) and SEM (900x, right) images of a PCL-SC and a PCL-ESP film.

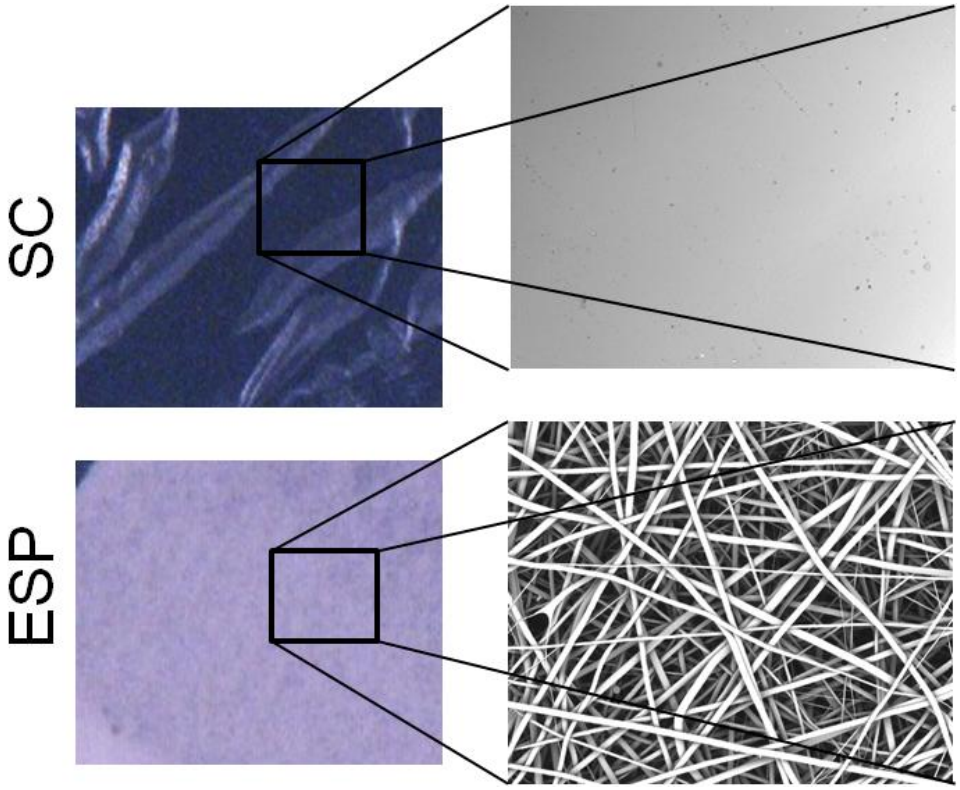

Figure 4: EPR spectra of (a) the empty rod, and of a PCL-ESP film (b) blank, (c) after a standard Ar-plasma treatment and subsequent exposure to air at RT for 10 minutes, and (d) after additional *in-situ* UV irradiation for 70 minutes at 20 K. All spectra were recorded on the same sample.

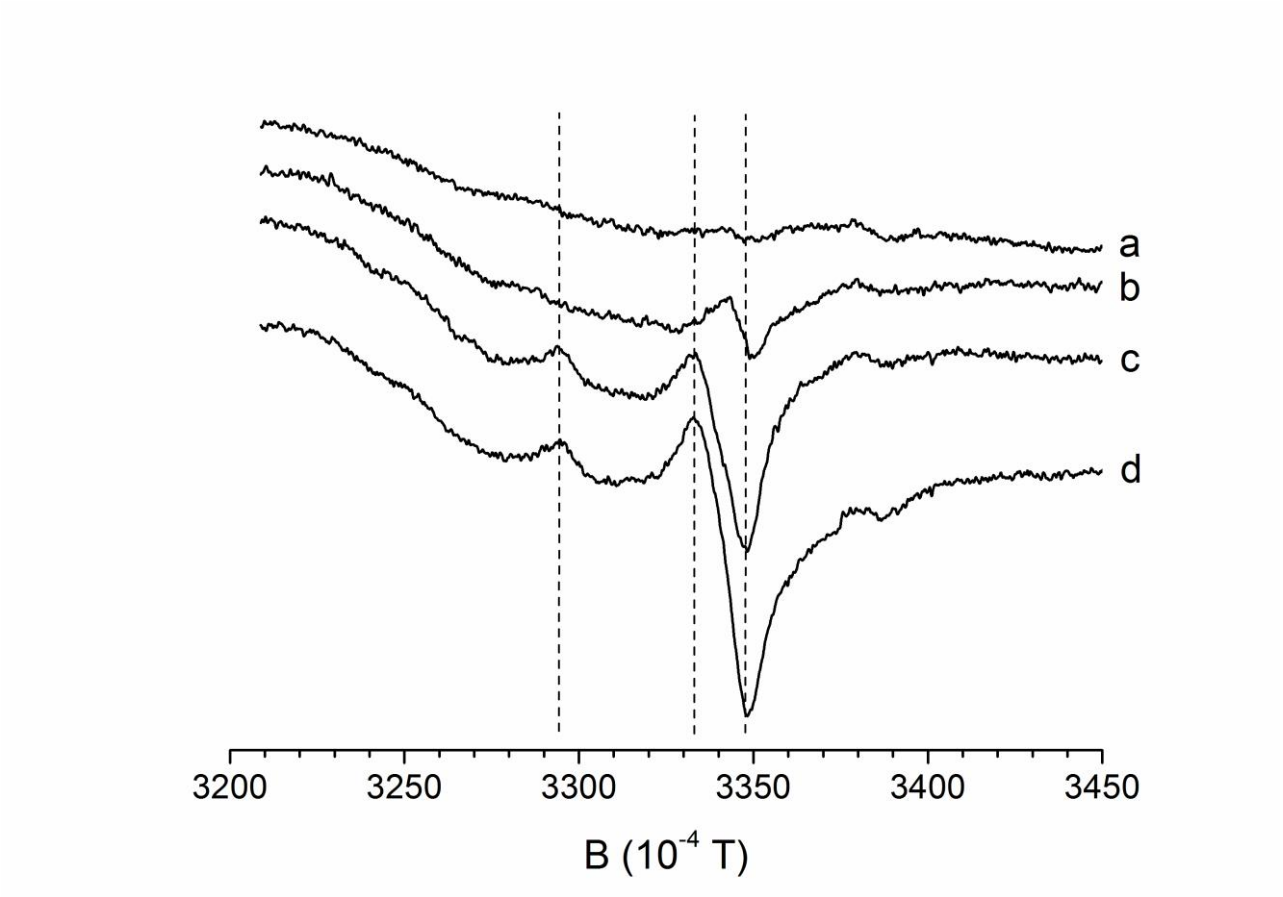

Figure 5: EPR spectra of (a) PCL-SC and (b) PCL-ESP films, subjected to the same Ar-plasma treatment and measured with identical EPR parameters settings. Spectrum a has been intensity-normalized by a factor 6.

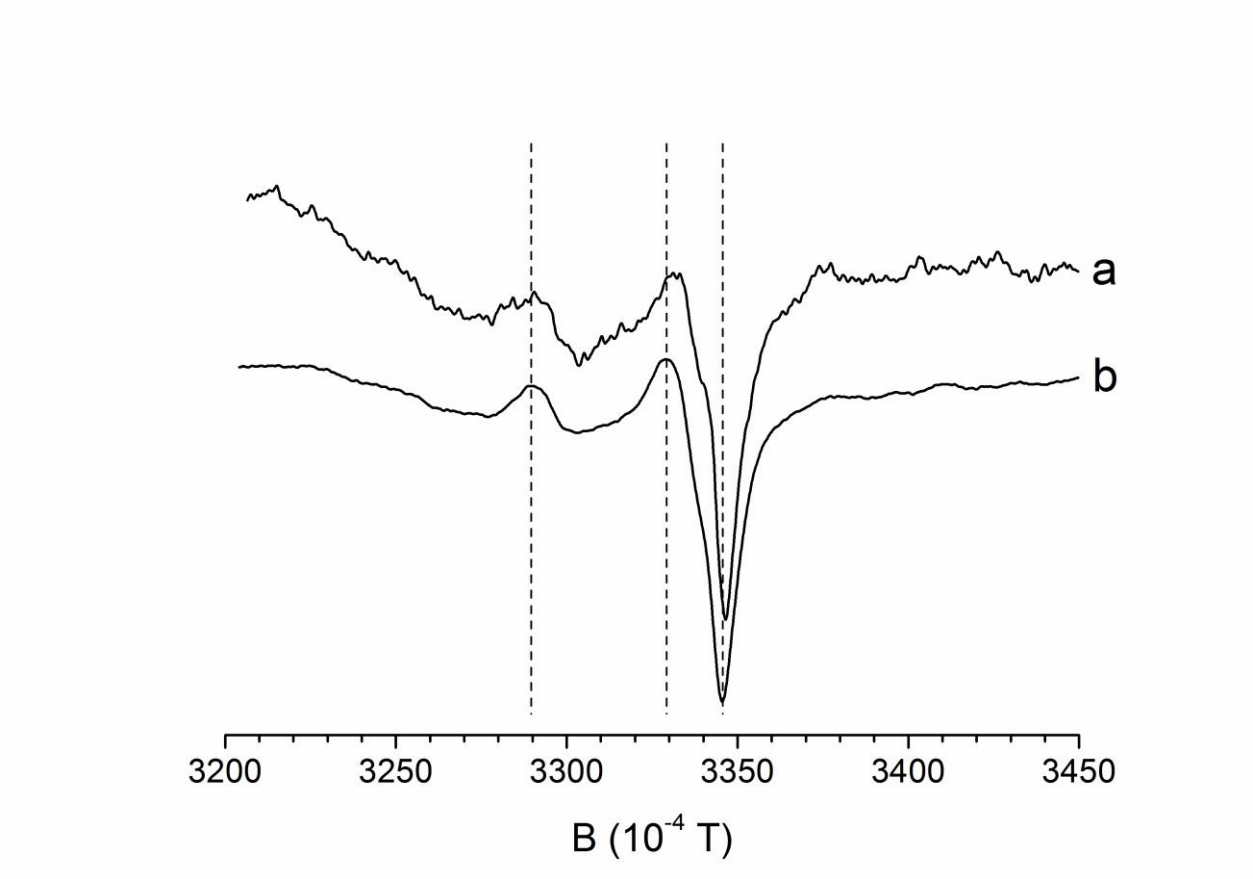

Figure 6: Experimental EPR spectra of (a) a blank and (b) an Ar-plasma-treated PCL-ESP film of comparable surface. Spectrum c is the plasma-induced EPR signal obtained by subtracting spectrum a from spectrum b. The red and green lines are simulated powder EPR spectra. The red spectrum was obtained assuming a single type of radical species with principal g values g_x = 2.0019, g_y = 2.0082 and g_z = 2.0347 and a Gaussian line profile with isotropic line broadening. For the green spectrum, anisotropic line broadening, strain on the g values and a combination of Gaussian and Lorentzian line profiles was used, with principal g values g_x = 2.0023, g_y = 2.0078 and g_z = 2.0347.

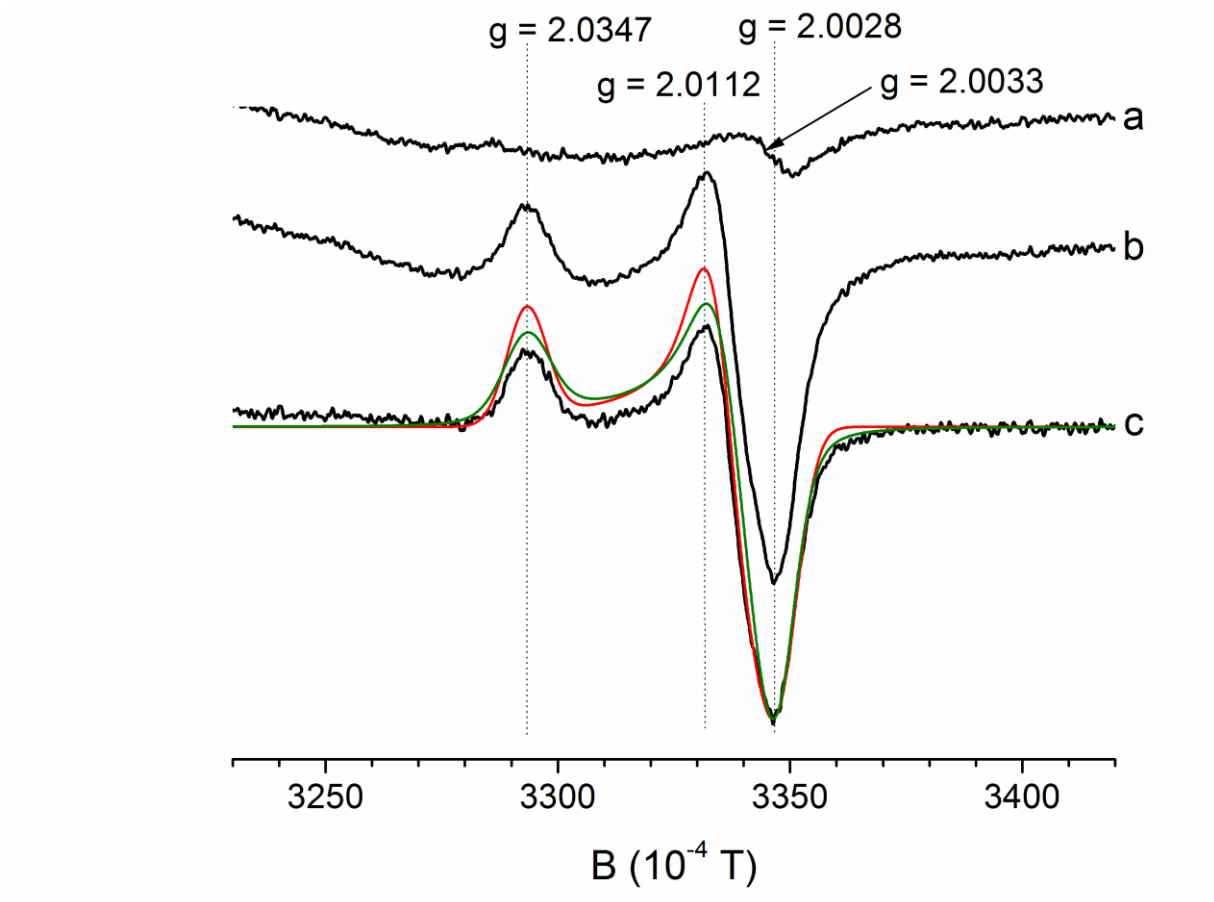

Figure 7: EPR spectra recorded for a PCL-ESP film (a) after a standard Ar-plasma treatment, (b) after subsequent *in-situ* (He atmosphere) annealing to RT for 20 minutes and (c) blank (i.e. before Ar-plasma treatment).

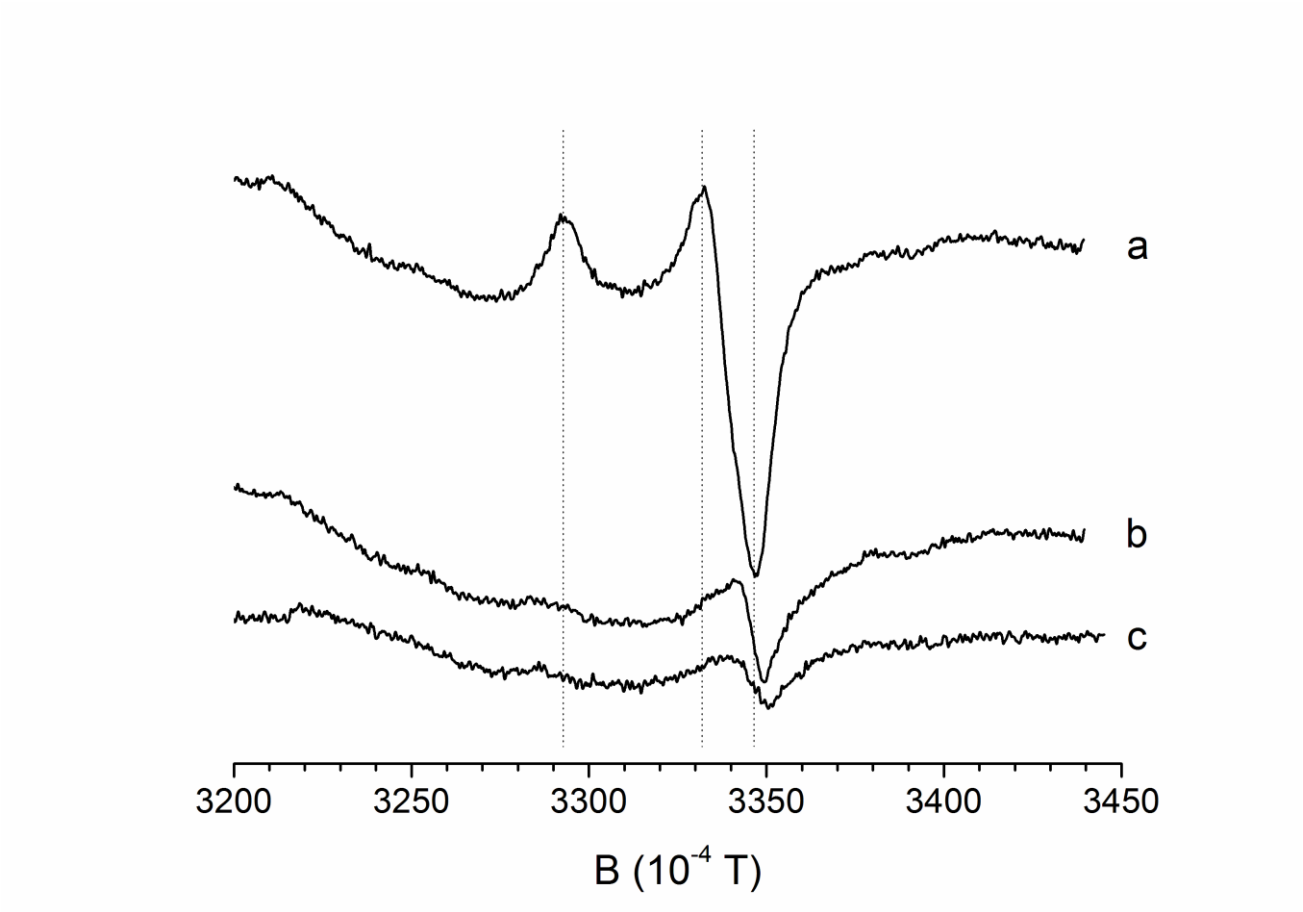

Figure 8: EPR spectra recorded on (a) a blank PCL-ESP film and (b) after 40 minutes *in-situ* UV irradiation at 20 K. Spectrum c is obtained by subtracting spectrum a from spectrum b. Spectrum d is a repetition of spectrum c in Figure 6, showing the Ar-induced signal in a comparable sample and recorded with identical parameter settings.

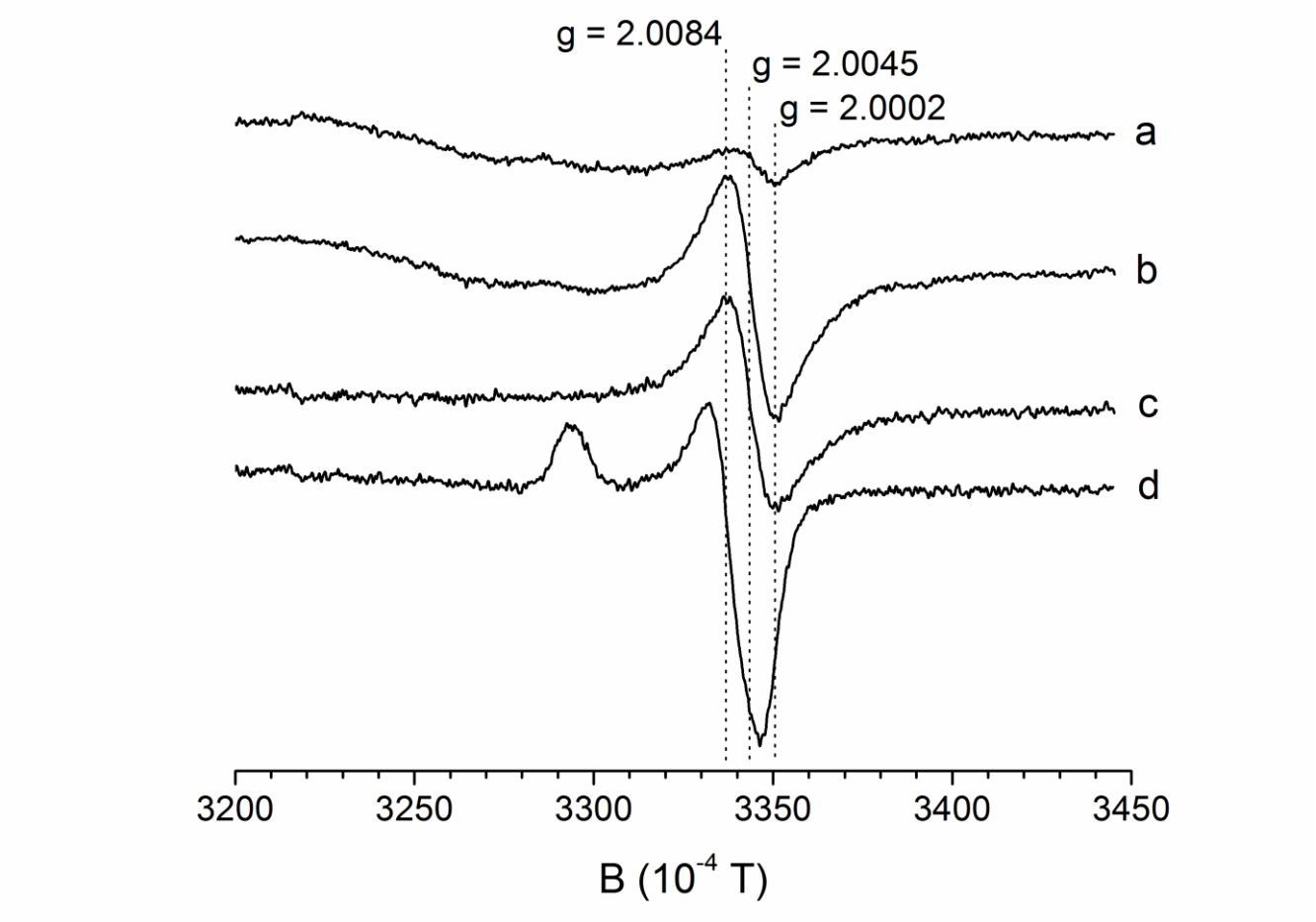

Figure 9: EPR spectra recorded on a standard Ar-plasma-treated PCL-ESP film (a) before and (b) after *in-situ* UV irradiation for 80 minutes at 20 K. Spectrum c is obtained by subtracting spectrum a from spectrum b. Spectrum d is an intensity-normalized repetition of spectrum c in Figure 8, and yields the EPR signal induced by 40 minutes *in-situ* UV radiation at 20 K of a comparable PCL-ESP film which has not undergone Ar-plasma treatment.

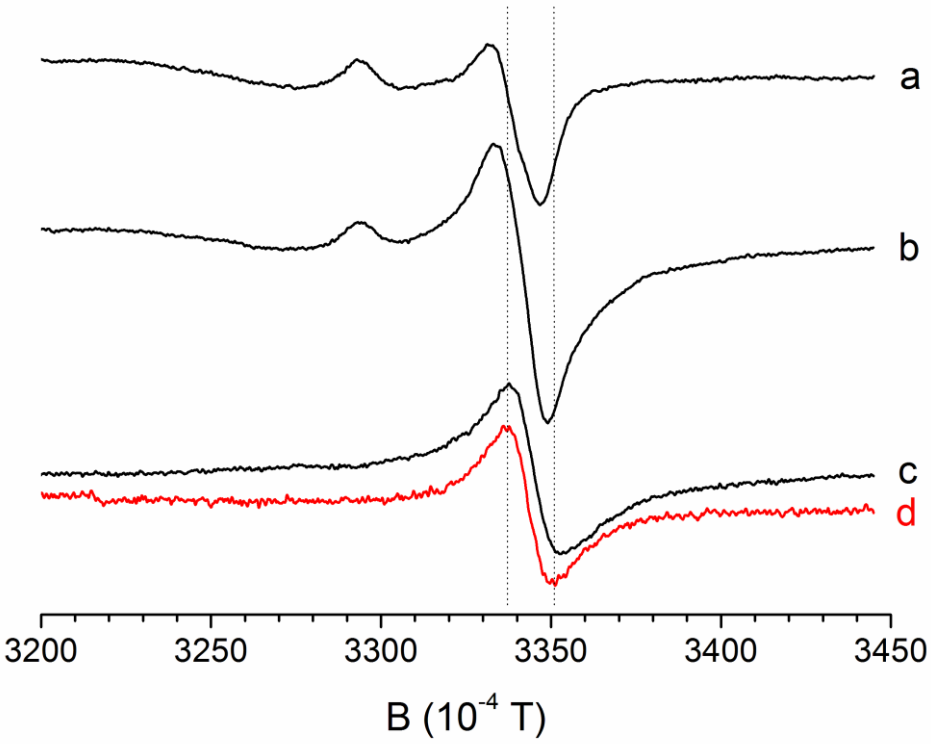

Graphical abstract

The EPR signals of radicals induced in electrospun PCL films by Ar plasma (red) or UV light (blue) during post-plasma grafting indicate the former are mainly oxygen-centered and the latter mainly carbon-centered. The UV generation of radicals appears to be independent of the plasma pre-treatment. This raises questions with respect to the molecular mechanisms generally assumed to underpin the post-plasma grafting process.